21st Australasian Fluid Mechanics Conference
Adelaide, Australia
10-13 December 2018

Size-dependent bifurcations of microtubes conveying fluid flow embedded in a nonlinear elastic medium

Ali Farajpour[1], Mergen H. Ghayesh[1] and Hamed Farokhi[2]

[1]School of Mechanical Engineering
University of Adelaide, South Australia 5005, Australia

[2]Department of Mechanical and Construction Engineering,
Northumbria University, Newcastle upon Tyne NE1 8ST, UK

Abstract

The size-dependent bifurcation behaviour of a fluid-conveying microtube taking into account the effect of internal energy loss is studied in this paper. It is assumed that the viscoelastic microscale tube is externally excited by a transverse harmonic force. In addition, the viscoelastic microscale system is surrounded by a nonlinear spring bed. To take into account the influence of the internal energy loss on the size-dependent bifurcation behaviour, the Kelvin-Voigt scheme of viscoelasticity is employed. The modified couple stress theory (MCST), as a size-dependent theory, and the Hamilton principle, as an energy/work law, are utilised for deriving the governing coupled equations for the bifurcation response of the viscoelastic fluid-conveying microtube. The displacement along the transverse direction as well as the axial displacement are incorporated into the size-dependent continuum model, leading to an accurate coupled continuum-based model. The Galerkin weighted-residual scheme, as a decomposition approach, is then applied to the derived nonlinear differential equations. Clamped-clamped boundary conditions are taken into consideration for extracting numerical results. The size-dependent bifurcation behaviour of the fluid-conveying viscoelastic microtube is finally predicted by a numerical time-integration technique.

Introduction

Fluid-structure interactions at microscale levels have recently been at the centre of attention of many scientific communities owing to the fact that some useful microscale devices such as microfluidics and microscale biosensors work based on these interactions [1, 2]. It is important to improve the knowledge level on the mechanical behaviour such as the bifurcation of fluid-conveying microscale structures under various external loads since in order to design a microscale system with fluid-structure interactions, the proper prediction of its time-dependent deformation is required.

Some modified elasticity models have been introduced to capture the size influence on the dynamic response of fluid-conveying small-scale structures. The most popular ones are the nonlocal theory [3-7], the couple stress model [8-10] and the nonlocal strain gradient elasticity [11, 12]. In this analysis, the modified couple stress theory (MCST) is applied since it is able to capture the size influence at microscale levels.

Although the dynamic response of fluid-conveying macroscale structures have been widely studied in the literature [13, 14], the number of research investigations on the mechanics of small-scale structures conveying flowing fluid is limited. Some of the most relevant investigations are concisely explained in the following. Wang [15] explored the linear scale-dependent oscillation of tubes containing fluid flow at microscale levels; he applied the MCST to capture the size influence. Kural and Özkaya [16] also studied the effect of an elastic foundation on the vibration of microscale beams conveying fluid; they utilised a perturbation technique to present an approximate solution. In addition, Dehrouyeh-Semnani et al. [17] examined the vibrational behaviour of micropipes containing fluid flow via an Euler–Bernoulli model together with the MCST; they took into consideration von Kármán's geometrical nonlinearity in the formulation. In another paper, Hosseini and Bahaadini [18] developed a scale-dependent theoretical model for analysing the stability of cantilever pipes containing fluid flow at microscale levels via a modified strain gradient model. Furthermore, a parametric size-dependent investigation was presented in the literature on the flow-induced time-dependent deformation of pipes with clamped-free ends [19]. Tang et al. [20] also investigated the large amplitude vibrational behaviour of curved microscale tube containing fluid flow via the MST. More lately, the effects of thermal stresses on the forced vibrational response of carbon nanotubes have been explored by Askari and Esmailzadeh [21]. Moreover, a nonlinear analysis has been reported on the flow-induced vibrational response of piezoelectric nanoscale tubes incorporating the influence of large deformations [22].

In this analysis, a scale-dependent continuum model is proposed to examine the bifurcation behaviour of a fluid-conveying microtube resting on a nonlinear elastic medium in the super critical regime. The influences of the geometrical nonlinearity and the internal energy loss as well as the size influences are incorporated in the continuum modelling and the solution method. It is assumed that the microtube is subject to transverse harmonic loading. Using the Kelvin-Voigt scheme, MCST and a Hamilton approach, the differential equations of motion are derived. Both two types of displacement components (i.e. the axial and transvers ones) are simultaneously considered in the scale-dependent nonlinear modelling. Galerkin's procedure was implemented in order to obtain a set of ordinary differential equations from the coupled partial differential equations of the microscale system. Finally, to solve the obtained ordinary differential equations, a continuation scheme is applied. Numerical results are presented for clamped-clamped microtubes in the supercritical regime.

Scale-dependent formulation

Figure 1 illustrates the schematic diagram of a microtube conveying fluid flow resting on a nonlinear elastic medium. The small-scale tube is subject to an excitation force given by $F(x)\cos(\omega t)$ where F denotes the forcing amplitude, and ω is the excitation frequency. The length of the microtube and the velocity of the fluid flow are denoted by L and U_f, respectively. The plug flow assumption is considered as the boundary layer thickness is negligible. Moreover, D_i and D are respectively the inner and outer diameters of the microscale tube.

Based on von Kármán's geometrical nonlinearity and the Euler-Bernoulli model of beams, one can write

$$\varepsilon_{xx}(x,z,t)=\sqrt{\left(\frac{\partial \hat{w}(x,t)}{\partial x}\right)^2+\left(1+\frac{\partial \hat{u}(x,t)}{\partial x}\right)^2}-1-z\frac{\partial \theta(x,t)}{\partial x}, \quad (1)$$

in which ε_{xx}, $\hat{w}$, $\hat{u}$ and θ represent the strain, transverse deflection, axial displacement and tube rotation, respectively. Taking into account the internal loss using Kelvin-Voigt viscoelasticity, the stress-strain relation is expressed as

$$\sigma_{xx}=\sigma_e+\sigma_v,\quad \begin{Bmatrix}\sigma_e\\ \sigma_v\end{Bmatrix}=\begin{Bmatrix}E\varepsilon_{xx}\\ \alpha\dfrac{\partial\varepsilon_{xx}}{\partial t}\end{Bmatrix}. \tag{2}$$

In the above relations (i.e. Eq. (2)), σ_{xx}, σ_e and σ_v are respectively the total, elastic and viscoelastic stresses; E and α indicate the elastic and viscosity constants of the microtube, respectively.

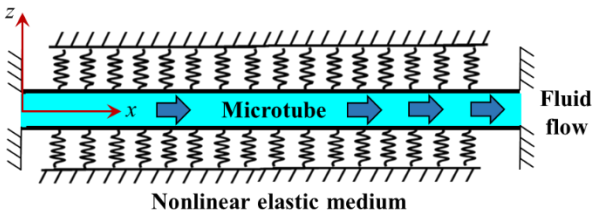

Figure 1. A microtube embedded in a nonlinear elastic medium conveying fluid flow.

Employing the MCST, the symmetric curvature (χ_{ij}) is related to the displacement components as follows

$$\begin{Bmatrix}\chi_{xy}\\ \chi_{yz}\end{Bmatrix}=-\frac{1}{4}\begin{Bmatrix}\dfrac{\partial\sin\theta}{\partial x}+\dfrac{\partial^2\hat{w}}{\partial x^2}\\ \dfrac{\partial\cos\theta}{\partial x}\end{Bmatrix}-\frac{z}{4}\begin{Bmatrix}\dfrac{\partial^2\cos\theta}{\partial x^2}\\ 0\end{Bmatrix}. \tag{3}$$

The deviatoric symmetric couple stress (m_{ij}) and the symmetric curvature are also related by the following relation

$$\begin{Bmatrix}m_{xy}\\ m_{yz}\end{Bmatrix}=\begin{Bmatrix}m_{xy(e)}\\ m_{yz(e)}\end{Bmatrix}+\begin{Bmatrix}m_{xy(v)}\\ m_{yz(v)}\end{Bmatrix},$$

$$\begin{Bmatrix}m_{xy(e)}\\ m_{yz(e)}\end{Bmatrix}=\frac{l^2E}{1+\nu}\begin{Bmatrix}\chi_{xy}\\ \chi_{yz}\end{Bmatrix},\quad \begin{Bmatrix}m_{xy(v)}\\ m_{yz(v)}\end{Bmatrix}=\frac{l^2\alpha}{1+\nu}\begin{Bmatrix}\dfrac{\partial\chi_{xy}}{\partial t}\\ \dfrac{\partial\chi_{yz}}{\partial t}\end{Bmatrix}, \tag{4}$$

where l denotes the scale parameter, and ν is Poisson's ratio. It should be noticed that "e" and "v" represent the elastic and viscoelastic segments of the corresponding tensor, respectively. Formulating the kinetic energy, elastic energy, external work, the work done due to the internal friction and the elastic energy of the nonlinear elastic medium, and then applying Hamilton's principle, the coupled nonlinear equations of the microtube are obtained. To obtain numerical results, first the derived equations are made dimensionless. Then, the equations are discretised using the following relations

$$\begin{Bmatrix}\bar{w}(\bar{x},\tau)\\ \bar{u}(\bar{x},\tau)\end{Bmatrix}=\begin{Bmatrix}\sum_{k=1}^{N_w}q_k(\tau)\bar{W}_k(\bar{x})\\ \sum_{k=1}^{N_u}r_k(\tau)\bar{U}_k(\bar{x})\end{Bmatrix}, \tag{5}$$

in which $\bar{x}=x/L$, $\bar{u}=\hat{u}/D$ and $\bar{w}=\hat{w}/D$ are respectively the dimensionless axial coordinate, axial displacement and transverse deflection. The dimensionless time is also denoted by $\tau=t\sqrt{EI/\left[L^4(M+m)\right]}$ where m, M and I indicate the tube mass per length, the fluid mass per length and the tube moment of inertia, respectively. The microbeam is composed of epoxy polymeric micromaterials. The detailed materials properties are described in the next section. (q_k,r_k) and ($\bar{W}_k$,$\bar{U}_k$) represent the generalised coordinates and shape functions, respectively. Applying Eq. (5), the derived equations can be written as

$$\begin{aligned}
&\sum_{j=1}^{N_u}J_{ij}^{(1,1)}\ddot{r}_j+2\sqrt{\beta}u_f\sum_{j=1}^{N_u}J_{ij}^{(1,2)}\dot{r}_j+\left(u_f^2-\Pi_0\right)\sum_{j=1}^{N_u}J_{ij}^{(1,3)}r_j\\
&-\frac{1}{S}\left(\frac{1}{2}\bar{\mu}+1\right)\sum_{j=1}^{N_w}\sum_{k=1}^{N_w}J_{ij}^{(1,4)}q_jq_k-\frac{\Pi_0}{S}\sum_{j=1}^{N_w}\sum_{k=1}^{N_w}J_{ij}^{(1,5)}q_jq_k\\
&-\Pi_0\alpha_v\sum_{j=1}^{N_u}J_{ij}^{(1,6)}\dot{r}_j-\frac{\Pi_0\alpha_v}{S}\sum_{k=1}^{N_w}\sum_{j=1}^{N_w}J_{ij}^{(1,7)}\left(\dot{q}_kq_j+q_k\dot{q}_j\right)\\
&-\frac{\alpha_v}{S}\left(\frac{1}{2}\bar{\mu}+1\right)\sum_{j=1}^{N_w}\sum_{k=1}^{N_w}J_{ij}^{(1,8)}q_j\dot{q}_k=0,\\
&\sum_{j=1}^{N_w}J_{ij}^{(2,1)}\ddot{q}_j+2\sqrt{\beta}u_f\sum_{j=1}^{N_w}J_{ij}^{(2,2)}\dot{q}_j+u_f^2\sum_{j=1}^{N_w}J_{ij}^{(2,3)}q_j\\
&+\left(1+\bar{\mu}\right)\sum_{j=1}^{N_w}J_{ij}^{(2,4)}q_j+\alpha_v\left(1+\bar{\mu}\right)\sum_{j=1}^{N_w}J_{ij}^{(2,5)}\dot{q}_j\\
&-\Gamma\sum_{j=1}^{N_w}J_{ij}^{(2,6)}q_j-\frac{\Pi_0}{S}\left[\frac{3}{2S}\sum_{k=1}^{N_w}\sum_{j=1}^{N_w}\sum_{l=1}^{N_w}J_{ij}^{(2,7)}q_kq_jq_l\right.\\
&\left.+\sum_{j=1}^{N_u}\sum_{k=1}^{N_w}J_{ij}^{(2,8)}r_jq_k\right]+K_1\sum_{j=1}^{N_w}J_{ij}^{(2,9)}q_j+K_2\sum_{k=1}^{N_w}\sum_{j=1}^{N_w}\sum_{l=1}^{N_w}J_{ij}^{(2,10)}q_kq_jq_l\\
&-\frac{1}{S}\left[\sum_{k=1}^{N_u}\sum_{j=1}^{N_w}J_{ij}^{(2,11)}r_kq_j+\frac{1}{S}\sum_{j=1}^{N_w}\sum_{k=1}^{N_w}\sum_{l=1}^{N_w}J_{ij}^{(2,12)}q_jq_kq_l\right]\\
&-\frac{\bar{\mu}}{4S}\left[\sum_{j=1}^{N_u}\sum_{k=1}^{N_w}J_{ij}^{(2,13)}r_jq_k+\frac{1}{S}\sum_{j=1}^{N_w}\sum_{k=1}^{N_w}\sum_{l=1}^{N_w}J_{ij}^{(2,14)}q_jq_kq_l\right]\\
&-\frac{\bar{\mu}}{4\Pi_0S^2}\sum_{j=1}^{N_w}\sum_{k=1}^{N_w}\sum_{l=1}^{N_w}J_{ij}^{(2,15)}q_jq_kq_l-\frac{\alpha_v\Pi_0}{S}\times\\
&\left[\frac{1}{S}\sum_{j=1}^{N_w}\sum_{k=1}^{N_w}\sum_{l=1}^{N_w}J_{ij}^{(2,16)}\left(2q_j\dot{q}_kq_l+q_jq_k\dot{q}_l\right)+\sum_{j=1}^{N_u}\sum_{k=1}^{N_w}J_{ij}^{(2,17)}\dot{r}_jq_k\right]\\
&-\frac{\alpha_v}{S}\left[\sum_{k=1}^{N_u}\sum_{j=1}^{N_w}J_{ij}^{(2,18)}\left(\dot{r}_kq_j+r_k\dot{q}_j\right)+\right.\\
&\sum_{k=1}^{N_u}\sum_{j=1}^{N_w}J_{ij}^{(2,19)}\left(3\dot{r}_kq_j+4r_k\dot{q}_j\right)+\sum_{k=1}^{N_u}\sum_{j=1}^{N_w}J_{ij}^{(2,20)}\left(\dot{r}_kq_j+2r_k\dot{q}_j\right)\\
&+\frac{1}{S}\sum_{j=1}^{N_w}\sum_{k=1}^{N_w}\sum_{l=1}^{N_w}J_{ij}^{(2,21)}\left(6\dot{q}_jq_kq_l+6q_j\dot{q}_kq_l+8q_jq_k\dot{q}_l\right)\\
&\left.+\frac{2}{S}\sum_{j=1}^{N_w}\sum_{k=1}^{N_w}\sum_{l=1}^{N_w}J_{ij}^{(2,22)}\left(\dot{q}_jq_kq_l+q_j\dot{q}_kq_l\right)+\frac{6}{S}\sum_{j=1}^{N_w}\sum_{k=1}^{N_w}\sum_{l=1}^{N_w}J_{ij}^{(2,23)}q_jq_k\dot{q}_l\right]\\
&-\frac{\bar{\mu}\alpha_v}{4S}\sum_{j=1}^{N_u}\sum_{k=1}^{N_w}J_{ij}^{(2,24)}\left(r_j\dot{q}_k+\dot{r}_jq_k\right)-\frac{\bar{\mu}\alpha_v}{4S}\sum_{j=1}^{N_u}\sum_{k=1}^{N_w}J_{ij}^{(2,25)}\left(4r_j\dot{q}_k+2\dot{r}_jq_k\right)\\
&-\frac{\bar{\mu}\alpha_v}{4S}\sum_{j=1}^{N_u}\sum_{k=1}^{N_w}J_{ij}^{(2,26)}\left(8r_j\dot{q}_k+6\dot{r}_jq_k\right)-\frac{4\bar{\mu}\alpha_v}{S^2}\sum_{j=1}^{N_w}\sum_{k=1}^{N_w}\sum_{l=1}^{N_w}J_{ij}^{(2,28)}q_jq_k\dot{q}_l\\
&-\frac{\bar{\mu}\alpha_v}{4S^2}\sum_{j=1}^{N_w}\sum_{k=1}^{N_w}\sum_{l=1}^{N_w}J_{ij}^{(2,27)}\left(17\dot{q}_jq_kq_l+15q_j\dot{q}_kq_l+20q_jq_k\dot{q}_l\right)\\
&-\frac{5\bar{\mu}\alpha_v}{4S^2}\sum_{j=1}^{N_w}\sum_{k=1}^{N_w}\sum_{l=1}^{N_w}J_{ij}^{(2,29)}\left(\dot{q}_jq_kq_l+q_j\dot{q}_kq_l\right)\\
&-\frac{\bar{\mu}\alpha_v}{4\Pi_0S^2}\sum_{j=1}^{N_w}\sum_{k=1}^{N_w}\sum_{l=1}^{N_w}J_{ij}^{(2,30)}\left(\dot{q}_jq_kq_l+6q_j\dot{q}_kq_l+5q_jq_k\dot{q}_l\right)\\
&-\frac{\bar{\mu}\alpha_v}{4\Pi_0S^2}\sum_{j=1}^{N_w}\sum_{k=1}^{N_w}\sum_{l=1}^{N_w}J_{ij}^{(2,31)}\left(q_jq_k\dot{q}_l+q_j\dot{q}_kq_l\right)
\end{aligned} \tag{6}$$

$$
\begin{aligned}
&-\frac{3\bar{\mu}\alpha_v}{2\Pi_0 S^2}\sum_{j=1}^{N_w}\sum_{k=1}^{N_w}\sum_{l=1}^{N_w} J_{ij}^{(2,32)} q_j q_k \dot{q}_l \\
&-\frac{5\bar{\mu}\alpha_v}{2\Pi_0 S^2}\sum_{j=1}^{N_w}\sum_{k=1}^{N_w}\sum_{l=1}^{N_w} J_{ij}^{(2,33)} \left(q_j q_k \dot{q}_l + q_j \dot{q}_k q_l\right) \\
&-\frac{\bar{\mu}\alpha_v}{\Pi_0 S^2}\sum_{j=1}^{N_w}\sum_{k=1}^{N_w}\sum_{l=1}^{N_w} J_{ij}^{(2,34)} \left(q_j \dot{q}_k q_l + q_j q_k \dot{q}_l\right) = 0,
\end{aligned} \tag{7}
$$

where $J_{ij}^{(k,lm)}$ are obtained using the Galerkin approach. In Eq. (6), i takes integer values from 1 to N_u while i varies from 1 to N_w in Eq. (7). Moreover, in these equations, the non-dimensional parameters are defined as

$$
\begin{aligned}
&\beta = \frac{M}{M+m},\ K_1 = \frac{k_1 L^4}{EI},\ K_2 = \frac{k_2 L^4 D^2}{EI}, \\
&\alpha_v = \frac{\alpha}{E}\sqrt{\frac{EI}{(M+m)L^4}},\ \Gamma = \frac{TL^2}{EI},\ \Pi_0 = \frac{AL^2}{I}, \\
&u_f = \sqrt{\frac{M}{EI}} U_f L,\ f_1 = \frac{F_1 L^4}{DEI},\ \bar{\mu} = \frac{Al^2}{2(1+\nu)I}, \\
&\Omega_e = \omega L^2 \sqrt{\frac{M+m}{EI}},\ S = \frac{L}{D},
\end{aligned} \tag{8}
$$

where k_1, k_2, A and T indicate the linear spring stiffness, nonlinear spring stiffness, cross-sectional area and pretension, respectively. A discretised system with 10 shape functions along each direction is taken into account. A backward differentiation formula is finally utilised to obtain the results.

Numerical results

A microtube conveying fluid flow embedded in a nonlinear elastic medium is taken into consideration. The material and geometrical properties are as ρ_{mt}=1220 kg/m^3, ρ_f=1000 kg/m^3, ν=0.38, E=1.44 GPa, D_i=30 μm, D=55 μm and L/D=100 where ρ_{mt} and ρ_f are respectively the microtube mass density and the fluid mass density [23]. In addition, unless clearly mentioned otherwise, the dimensionless parameters of the microscale system conveying fluid flow are set to Γ=5.0, Ω_e/ω_1=1, β=0.2577, α_v=0.0002, $\bar{\mu}$=0.4575, S=100, Π_0=1.2331×10^5, K_1=50 and K_2=50.

Figure 2 shows the bifurcation plots of microscale fluid-conveying tubes for the transverse motion (q_1) in the supercritical regime. The dimensionless speed of the fluid flow is set to u_f=8.2. The critical speed of the fluid flow related to divergence is 8.1446. From the figure, it can be seen that as the forcing amplitude increases, the microscale fluid-conveying tube undergoes many changes in terms of the dynamic behaviour. Many motion types including period-1, period-2, period-5 and chaos are observed. It implies that near the critical speed, the nonlinear dynamic behaviour of microscale fluid-conveying tubes is very sensitive to the forcing amplitude. For instance, in figure 3, the phase-plane portrait of the period-5 motion found in figure 2 at f_1=11 is plotted.

In figure 4, the bifurcation plots of microscale fluid-conveying tubes in the supercritical regime for the transverse motion (q_1) are plotted; the fluid speed is set to u_f=8.3. The influence of a slight increase in the speed of the fluid flow is examined. Again, a diversity of motion types is found for the microscale fluid-conveying tube. Nonetheless, a slight increase in the speed of the fluid flow perceptibly reduces the complexity of the dynamic behaviour as well as its diversity in the supercritical regime. Moreover, it is found that the last chaotic region of the microscale fluid-conveying tube shifts to the right (near f_1=60) with slightly increasing the fluid speed. In addition, to give more details about the first chaotic motion found in figure 4 (at f_1=2.7), the phase-plane portrait is illustrated in figure 5 for this scale-dependent motion.

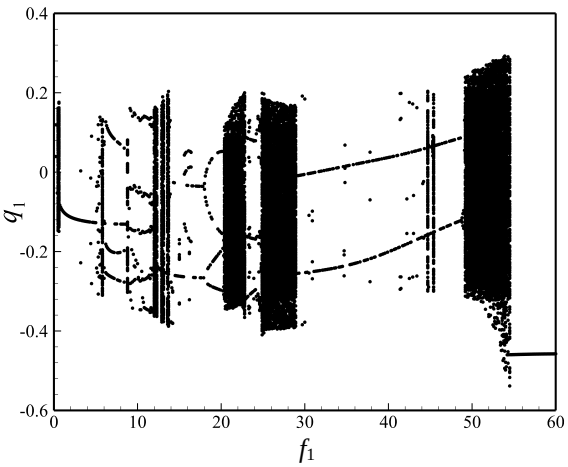

Figure 2. Bifurcation plots of microscale fluid-conveying tubes for q_1 in the supercritical regime for u_f=8.2.

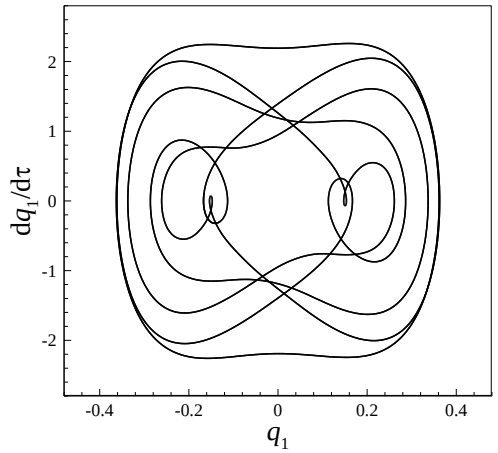

Figure 3. Phase-plane portrait of the period-5 motion found in figure 2 at f_1=11.

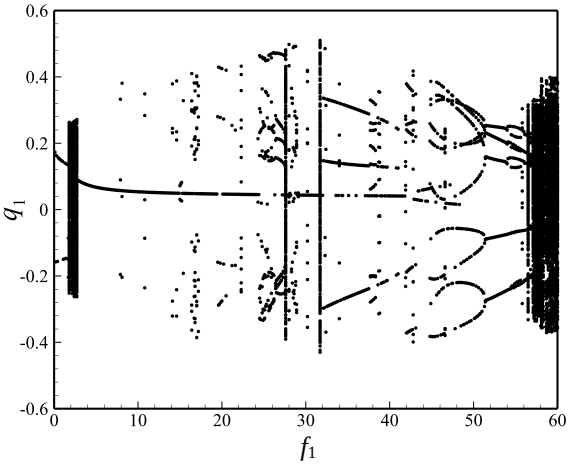

Figure 4. Bifurcation plots of microscale fluid-conveying tubes for q_1 in the supercritical regime for u_f=8.3.

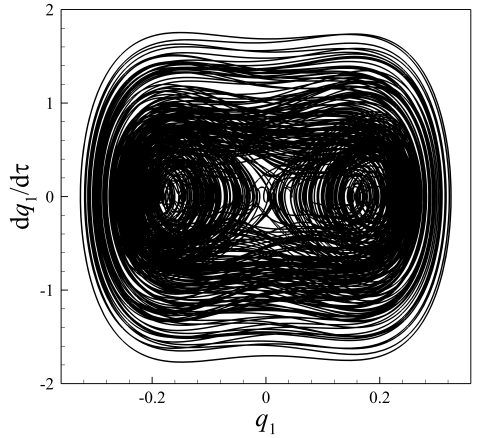

Figure 5. Phase-plane portrait of the chaotic motion found in figure 4 at f_1=2.7.

Conclusions

The bifurcation response of microscale fluid-conveying tubes was studied with consideration of the effect of internal energy loss. The microscale fluid-conveying tube was externally excited by a harmonic load along the transverse direction. Furthermore, the microscale tube was surrounded by a nonlinear elastic medium. The MCST, as a size-dependent continuum approach, Hamilton's approach, as an energy/work principle and Galerkin's scheme as a discretisation approach were applied for deriving a set of nonlinear coupled equations for the microscale fluid-conveying tube. The bifurcation of the microscale fluid-conveying tube in the supercritical regime was predicted by a time-integration technique.

It was found that as the forcing amplitude increases, the microscale fluid-conveying tube undergoes many changes in the nonlinear dynamic behaviour in the supercritical regime. Close to the critical speed, the nonlinear dynamic behaviour of microscale fluid-conveying tubes is very sensitive to the forcing amplitude of the excitation harmonic load. In the supercritical regime, a slight increase in the speed of the fluid flow decreases the complexity of the dynamic behaviour. Furthermore, a slight increase in the fluid speed makes the last chaotic region of the microscale system occur at higher forcing amplitudes.

References

[1] Warkiani ME, Guan G, Luan KB, Lee WC, Bhagat AAS, Chaudhuri PK, et al. Slanted spiral microfluidics for the ultra-fast, label-free isolation of circulating tumor cells. Lab on a Chip. 2014;14:128-37.
[2] Warkiani ME, Tay AKP, Khoo BL, Xiaofeng X, Han J, Lim CT. Malaria detection using inertial microfluidics. Lab on a Chip. 2015;15:1101-9.
[3] Reddy J. Nonlocal theories for bending, buckling and vibration of beams. International Journal of Engineering Science. 2007;45:288-307.
[4] Farajpour M, Shahidi A, Farajpour A. A nonlocal continuum model for the biaxial buckling analysis of composite nanoplates with shape memory alloy nanowires. Materials Research Express. 2018;5:035026.
[5] Aydogdu M. A nonlocal rod model for axial vibration of double-walled carbon nanotubes including axial van der Waals force effects. Journal of Vibration and Control. 2015;21:3132-54.
[6] Farajpour M, Shahidi A, Hadi A, Farajpour A. Influence of initial edge displacement on the nonlinear vibration, electrical and magnetic instabilities of magneto-electro-elastic nanofilms. Mechanics of Advanced Materials and Structures. 2018:1-13.
[7] Malekzadeh P, Farajpour A. Axisymmetric free and forced vibrations of initially stressed circular nanoplates embedded in an elastic medium. Acta Mechanica. 2012:1-20.
[8] Ma H, Gao X-L, Reddy J. A microstructure-dependent Timoshenko beam model based on a modified couple stress theory. Journal of the Mechanics and Physics of Solids. 2008;56:3379-91.
[9] Şimşek M. Dynamic analysis of an embedded microbeam carrying a moving microparticle based on the modified couple stress theory. International Journal of Engineering Science. 2010;48:1721-32.
[10] Farokhi H, Ghayesh MH. Nonlinear dynamical behaviour of geometrically imperfect microplates based on modified couple stress theory. International Journal of Mechanical Sciences. 2015;90:133-44.
[11] Lim C, Zhang G, Reddy J. A higher-order nonlocal elasticity and strain gradient theory and its applications in wave propagation. Journal of the Mechanics and Physics of Solids. 2015;78:298-313.
[12] Farajpour M, Shahidi A, Tabataba'i-Nasab F, Farajpour A. Vibration of initially stressed carbon nanotubes under magneto-thermal environment for nanoparticle delivery via higher-order nonlocal strain gradient theory. The European Physical Journal Plus. 2018;133:219.
[13] Païdoussis MP, Issid N. Dynamic stability of pipes conveying fluid. Journal of sound and vibration. 1974;33:267-94.
[14] Ghayesh MH, Païdoussis MP, Modarres-Sadeghi Y. Three-dimensional dynamics of a fluid-conveying cantilevered pipe fitted with an additional spring-support and an end-mass. Journal of sound and vibration. 2011;330:2869-99.
[15] Wang L. Size-dependent vibration characteristics of fluid-conveying microtubes. Journal of Fluids and Structures. 2010;26:675-84.
[16] Kural S, Özkaya E. Size-dependent vibrations of a micro beam conveying fluid and resting on an elastic foundation. Journal of Vibration and Control. 2017;23:1106-14.
[17] Dehrouyeh-Semnani AM, Nikkhah-Bahrami M, Yazdi MRH. On nonlinear vibrations of micropipes conveying fluid. International Journal of Engineering Science. 2017;117:20-33.
[18] Hosseini M, Bahaadini R. Size dependent stability analysis of cantilever micro-pipes conveying fluid based on modified strain gradient theory. International Journal of Engineering Science. 2016;101:1-13.
[19] Dehrouyeh-Semnani AM, Zafari-Koloukhi H, Dehdashti E, Nikkhah-Bahrami M. A parametric study on nonlinear flow-induced dynamics of a fluid-conveying cantilevered pipe in post-flutter region from macro to micro scale. International Journal of Non-Linear Mechanics. 2016;85:207-25.
[20] Tang M, Ni Q, Wang L, Luo Y, Wang Y. Nonlinear modeling and size-dependent vibration analysis of curved microtubes conveying fluid based on modified couple stress theory. International Journal of Engineering Science. 2014;84:1-10.
[21] Askari H, Esmailzadeh E. Forced vibration of fluid conveying carbon nanotubes considering thermal effect and nonlinear foundations. Composites Part B: Engineering. 2017;113:31-43.
[22] Saadatnia Z, Esmailzadeh E. Nonlinear harmonic vibration analysis of fluid-conveying piezoelectric-layered nanotubes. Composites Part B: Engineering. 2017;123:193-209.
[23] Lam DC, Yang F, Chong A, Wang J, Tong P. Experiments and theory in strain gradient elasticity. Journal of the Mechanics and Physics of Solids. 2003;51:1477-508.